International Journal of Pharmaceutics 446 (2013) 153–159

Contents lists available at SciVerse ScienceDirect

International Journal of Pharmaceutics

journal homepage: www.elsevier.com/locate/ijpharm

Pharmaceutical nanotechnology

A pH-responsive nano-carrier with mesoporous silica nanoparticles cores and poly(acrylic acid) shell-layers: Fabrication, characterization and properties for controlled release of salidroside

Hailong Peng[a,b], Ruichen Dong[a], Shenqi Wang[a], Zhong Zhang[c], Mei Luo[a,b], Chunqing Bai[a], Qiang Zhao[a], Jinhua Li[c], Lingxin Chen[c], Hua Xiong[a,*]

[a] State Key Laboratory of Food Science and Technology, Nanchang University, Nanchang 330047, China
[b] Department of Chemical Engineering, Nanchang University, Nanchang 330031, China
[c] Key Laboratory of Coastal Zone Environmental Processes, Yantai Institute of Coastal Zone Research, Chinese Academy of Sciences, Yantai 264003, China

ARTICLE INFO

Article history:
Received 28 October 2012
Received in revised form
17 December 2012
Accepted 30 January 2013
Available online 7 February 2013

Keywords:
Mesoporous silica nanoparticles
Poly(acrylic acid)
pH-responsive
Controlled release
Salidroside

ABSTRACT

A novel pH-responsive nano-carrier MSNs–PAA, possessing mesoporous silica nanoparticles (MSNs) cores and poly(acrylic acid) (PAA) shell-layers, was developed for controlled release of salidroside. The vinyl double bonds modified MSNs were synthesized by using cetyltrimethylammonium bromide (CTAB) as templates, tetraethyl orthosilicate (TEOS) as silicon source, and 3-(trimethoxylsilyl) propyl methacrylate (MPS) as surface modification functionalities. The pH-responsive layers of PAA were grafted onto the vinyl double bonds of the MSNs via precipitation polymerization, producing the MSNs–PAA with a hollow cubic core and mesoporous shell with penetrating pore channels. The characteristic results also showed that PAA was successfully grafted onto the surface of the MSNs. The MSNs–PAA was investigated as carriers for loading and regulating the release of salidroside in different pH solutions for the first time. The results demonstrated that the PAA layers on the surface of MSNs–PAA exhibited opened and closed states at different pH values, and thus could regulate the uptake and release of salidroside. The application of such pH-responsive nano-carrier might offer a potential platform for controlled delivery and increasing the bioavailability of drugs.

1. Introduction

Salidroside, a kind of physiologically active substance as well as one of the most potent pharmaceutical ingredients extracted from plants of the genus *Rhodiola rosea*, has long been actively used in medical practice (Rodin et al., 2012). It has exhibited a wide range of pharmacological properties, including anti-aging, anti-oxidation, anti-inflammatory, anti-fatigue, anti-depressant activities, antiviral effects, hepatoprotective, neuroprotective, and cardiovascular protective characteristics (Zhang et al., 2007, 2010; Wang et al., 2009). Recent studies have also shown that salidroside may prevent the growth of leukemia, stomach adenocarcinoma and parotid carcinoma (Hu et al., 2010), and may also significantly decrease neovascular reactions (De Bock et al., 2004). Despite its attractive pharmacological activities, the therapeutic potential of salidroside has been significantly restricted by its short biological half-life and poor oral bioavailability (Fan et al., 2007). To solve these drawbacks, organic-based carriers of liposomes and microspheres have been developed to encapsulate salidroside (Fan et al., 2007). However, these organic carriers often suffer from various disadvantages of instability in vivo/vitro environments, poor controlled release profile and usually leaking of entrapped components in water (Slowing et al., 2007, 2008; Fathi et al., 2012). Thus, formulating novel inorganic materials-based nano-carriers for encapsulation of salidroside may be one effective approach to overcome the above-mentioned problems.

Mesoporous silica nanoparticles (MSNs) have received great attention in the last few years, and have been intensively applied in biosensors (Hasanzadeh et al., 2012; Wang et al., 2011a), bio-markers (Lin et al., 2011), and chemical reactors (Tasbihi et al., 2011). Especially, MSNs have been recognized as a potential nano-carriers for bioactive molecules because of its biocompatibility and low cytotoxicity, stable mesoporous structure with large surface area, high porosity, adjustable pore diameter, and modifiable surface properties (Thomas et al., 2010; Tang et al., 2011). MSNs could selectively host guest molecules of various sizes, shapes and functionalities, such as drugs, genes, DNAs and proteins (Park et al., 2008; Lin et al., 2012; Giri et al., 2005). Compared to the most general organic carriers, MSNs have the significant advantage of being free from various biochemical attacks and bioerosions.

* Corresponding author. Tel.: +86 791 6634810; fax: +86 791 6634810.
E-mail address: huaxiong100@yahoo.com.cn (H. Xiong).

0378-5173/$ – see front matter © 2013 Elsevier B.V. All rights reserved.
http://dx.doi.org/10.1016/j.ijpharm.2013.01.071

However, the loading bioactive molecules would burst release from the unmodified MSNs, and could not release in a controllable manner to precisely match the actual physiological needs at the proper time/site (Kim et al., 2011a,b; Gao et al., 2010). All this disadvantages limit the applications of the unmodified MSNs as a novel nano-carrier.

For overcoming these disadvantages, stimuli-responsive MSNs have been developed by capping the pores using pH responsive materials (Nguyen et al., 2007; Leung et al., 2006; Taillefer et al., 2000) and temperature responsive polymers (You et al., 2008), quantum dots (Lai et al., 2003), iron oxide nanoparticles (Kim et al., 2011a,b) and gold nanoparticles (Torney et al., 2007; Wang et al., 2011a,b). Among all the triggers, pH-responsive MSNs have attracted special interest since each segment of organ maintains its own characteristic pH level (Dai et al., 2012). As is also well known that, the pH values are different between normal and abnormal tissues (Dai et al., 2012; Wang et al., 2010). The different pH environments have been used to design drug delivery systems. Meanwhile, pH-responsive materials are considered to be the best candidates for developing pH-responsive nano-carriers, which could be controlled and targeted release of drugs at the specific action sites (Fleige et al., 2012). On the other hand, pH-responsive nano-carriers could improve the stability of drugs. Thus, it is very important to develop ideal pH-responsive materials.

The polymer of poly(acrylic acid) (PAA) contains carboxylic groups that can release protons at high pH, and its solubility and structure are very sensitive to pH (Cui et al., 2012; Liu et al., 2006). PAA has good solubility at high pH values ($pH \geq 8$), however it has poor solubility and even collapses entangled together to precipitate from solution at low pH values ($pH \leq 4.0$) (Hong et al., 2009). PAA has other properties of forming a well-known bioadhesive hydrogel, sticking to the mucosal lining of the upper small intestine and protecting some protein drugs from degradation (Song et al., 2007). MSNs have been modified with PAA by layer-by-layer adsorption technique (Song et al., 2007) and "graft to" strategy of reversible addition-fragmentation chain transfer (RAFT) (Hong et al., 2009).

However, the above two modified techniques suffer from shortcomings of the irreversibility of the pore opening for layer-by-layer adsorption technique, and the relative tedious multiple-step syntheses for the "graft to" strategy (Fleming et al., 2001). Excitingly, seed polymerization strategy is an effective alternative to prepare microspheres with a core–shell structure (Jones and Lyon, 2000; Xu et al., 2011; Zhang et al., 2012). Therefore, it can be expected that the seed polymerization strategy can be applied to develop pH-responsive core–shell structured nano-carriers. However, to the best of our knowledge, the coating of pH-responsive polymers of PAA onto MSNs via seed polymerization is rarely mentioned.

In the present study, we describe for the first time the successful fabrication of novel pH-responsive nano-carriers (MSNs–PAA) with PAA layers and MSNs cores via seeded precipitation polymerization. Salidroside was selected as drug model for investigating the uptake and delivery behaviors of MSNs–PAA. The physicochemical characteristics, loading capacity and in vitro release properties of MSNs–PAA were also investigated.

2. Materials and methods

2.1. Materials

Salidroside was purchased from National Institutes for Food and Drug Control (Beijing, China). Tetraethylorthosilicate (TEOS), cetyltrimethylammonium bromide (CTAB), and *N*, *N*′-methylene bisacrylamide (MBA) were purchased from Aladdin (Shanghai, China). 3-(Trimethoxylsilyl) propyl methacrylate (MPS) and acrylic acid (AA) were obtained from Sigma–Aldrich (Shanghai, China). Other affiliated chemicals were all obtained from Donghu Chemical Reagents Co. (Nanchang, China). The deionized water used was produced by a Milli-Q Ultrapure water system with the water outlet operating at 18.2 MΩ cm specific resistance (Millipore, Bedford, MA, USA).

2.2. MPS coated MSNs (MSNs-MPS)

Silica nanoparticles with CTAB (SN-CTAB) were synthesized according to the sol–gel method (Slowing et al., 2007). Thereafter, the obtained SN-CTAB (500.0 mg) was dispersed into anhydrous ethanol (150 mL) followed by addition of MPS (10 mL). The mixture reacted for 48 h and the vinyl double bonds were formed on the surface of SN-CTAB. The resultants were isolated by filtration and washed with acetic acid for removing of unreacted MPS. Finally, CTAB was removed by refluxing in an ethanol solution of hydrochloric acid (HCl, 0.37%) for 48 h. The product of MSNs-MPS was then filtrated, washed and dried under vacuum.

2.3. Growing pH-responsive layers onto the surface of MSNs

MSNs–MPS (0.30 g) was dispersed into deionized water (60.0 mL), and AA (0.70 g) was then added into the solution. The mixture was stirred at 80 °C for 60 min under a nitrogen flow. Then, the cross-linker of MBA (130.0 mg) and the initiator of $K_2S_2O_8$ (60.0 mg) were added and reacted for 6 h at 70 °C under a nitrogen flow. The resulting products of MSNs–PAA were obtained by centrifuging and washed with deionized water.

2.4. Characterization

Fourier transform infrared (FT-IR) spectra were recorded by using the FT-IR spectrophotometer (Nicolet 5700, Thermo Electron Corporation, MA, USA). Thermal gravimetric analyses (TGA) were carried out on a differential scanning calorimeter (SDT-Q-600, TGA-DSC, TA instruments, USA) with a heating rate of 5 °C min^{-1} under nitrogen environment. The low angel X-ray diffractometer (XRD) patterns were recorded using XRD analyzer (D8-FOCUS, Bruker, Karlsruhe, Germany) with the scattering angle (2θ) range of 1–10°. Scanning electron microscopy (SEM) (Quanta 200F, FEI, Hillsboro, OR, USA) images were taken with an energy-dispersive X-ray spectrum (EDS). Size distribution was determined by Zetasizer Nonao-ZS (PSA NANO2590, Malvern Instruments, UK). Transmission electron microscopy (TEM) images were obtained on a JEOL (JEM-2010HR, Japan) transmission electron microscope. N_2 adsorption-desorption isotherms and structure parameters (surface area, pore size and volume) were obtained with Beishide instruments (3H-2000, Beijing, China).

2.5. Encapsulation efficiency and loading capacity

MSNs–PAA (20.0 mg) was dispersed into a solution of salidroside (0.25 mg/mL) in PBS buffer solutions (5.0 mL) with stirring at room temperature for 48 h. MSNs–PAA were collected by centrifugation and washed with PBS solution for 3 times. The mass of salidroside loaded into MSNs–PAA was calculated by subtracting the mass of salidroside in the supernatant from the total mass in the initial solution with HPLC methods at 275 nm. The loading content (LC) and entrapment efficiency (EE) were calculated according to the following equations:

$$LC(\%) = \frac{\text{Mass of salidroside in MSNs–PAA}}{\text{Mass of MSNs–PAA}} \times 100\% \quad (1)$$

$$EE(\%) = \frac{\text{Mass of salidroside in MSNs–PAA}}{\text{Initial mass of salidroside}} \times 100\% \quad (2)$$

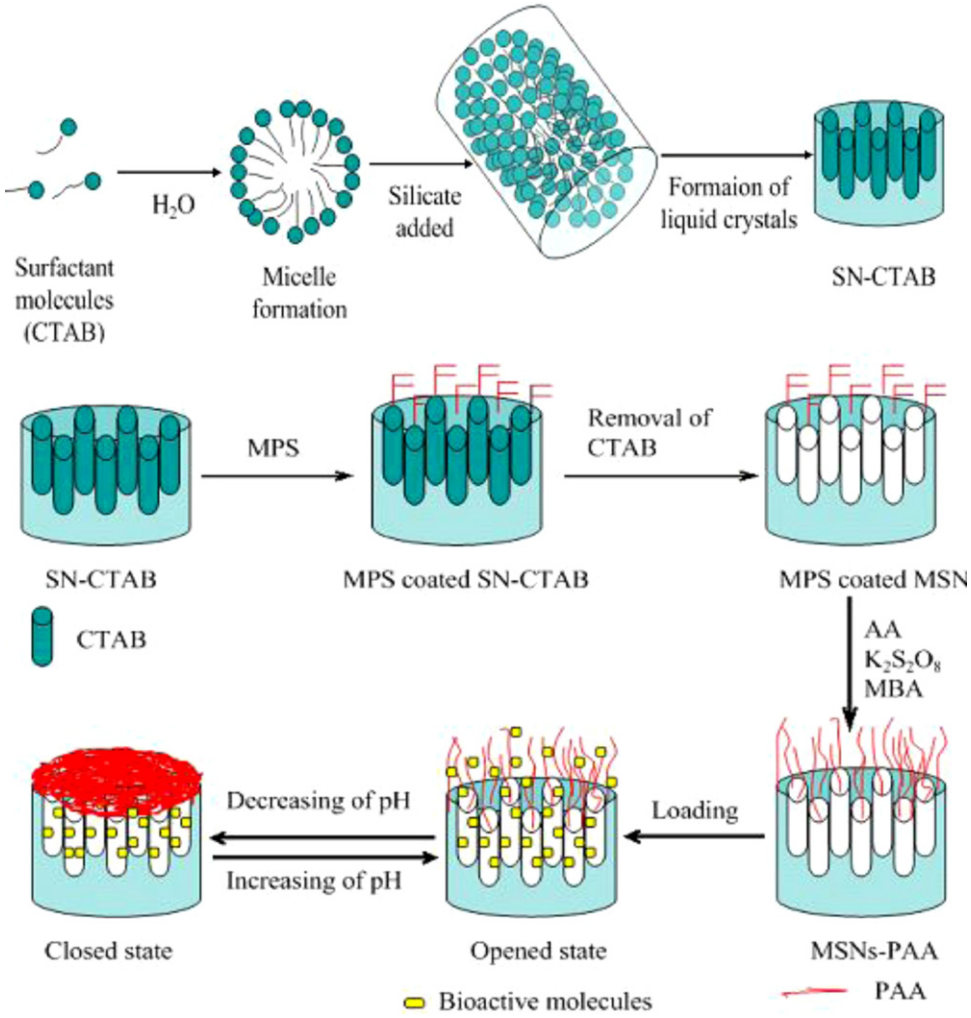

Fig. 1. Schematic illustration of the synthetic procedure for MSNs–PAA. SN-CTAB: silica nanoparticle with CTAB; MPS: 3-(trimethoxylsilyl) propyl methacrylate; CTAB: cetyltrimethylammonium bromide; TEOS: tetraethylorthosilicate; PAA: poly(acrylic acid); MBA: *N*, *N*′-methylene bisacrylamide; bioactive materials: salidroside.

2.6. In vitro release

The loaded MSNs–PAA samples (20.0 mg) were dispersed into 10.0 mL of PBS (pH 1.2 or pH 8.0) and gently shaken at 37.0 °C. At predetermined time, the PBS solution (1.0 mL) were withdrawn and replaced with equal volume of the corresponding fresh media to maintain a constant volume. The amount of released salidroside was analyzed by HPLC. In order to gain insight into the release mechanism of salidroside from MSNs–PAA, the release data were fitted according to Peppas model as following equation.

$$\text{Peppas model}: \ln \frac{M_t}{M_\infty} = n \ln t + \ln k \quad (3)$$

where M_t/M_∞ is the fractional release of salidroside at time t, n gives an indication of the release mechanism.

3. Results and discussion

3.1. Fabrication of pH-responsive MSNs (MSNs–PAA)

Fig. 1 illustrates the preparation process of MSNs–PAA. Due to the hydrophobic tails tend to congregate and their hydrophilic heads provide protection, the surfactants of CTAB would be clustered together and formed micelles in water. After that, the inorganic species (TEOS) were introduced into the micelles solutions and then the SN-CTAB was synthesized according to the sol–gel method (Slowing et al., 2007). Subsequently, the surface of SN-CTAB was modified with MPS and C=C grated onto the surface of SN-CTAB. Since the SN was filled with CTAB, double bonds were only grafted onto the exterior surface of SN-CTAB. And then, the modified SN-CTAB was refluxed in ethanol solutions of HCl, and the CTAB inside the SN was removed and yielded mesoporous silica nanoparticles (MSNs) with double bonds on the exterior surface. Finally, the MSNs–PAA could be developed by seeded precipitation polymerization using modified MSNs as seeds, $K_2S_2O_8$ as initiator, MBA as cross-linker, and AA as monomer and thereby forming pH-responsive material of PAA on the surface of MSNs.

3.2. Characterization of the pH-responsive MSNs (MSNs–PAA)

The ordered mesoporous structure of the MSNs was investigated by small angle XRD measurement and the results are shown in Fig. 2. Three well-resolved diffraction peaks, assigned as (1 0 0), (1 1 0) and (2 0 0) planes, could be clearly observed in the XRD pattern of MSNs, which come from the typical peaks of MCM-41. The results indicated that the MSNs had typical and ordered mesoporous structure like MCM-41. After modification with AA, there was a relatively weak diffraction peak (1 0 0), accompanied by the loss of the (1 1 0) and (2 0 0) reflections, indicating PAA layers fully covered the surface of MSNs.

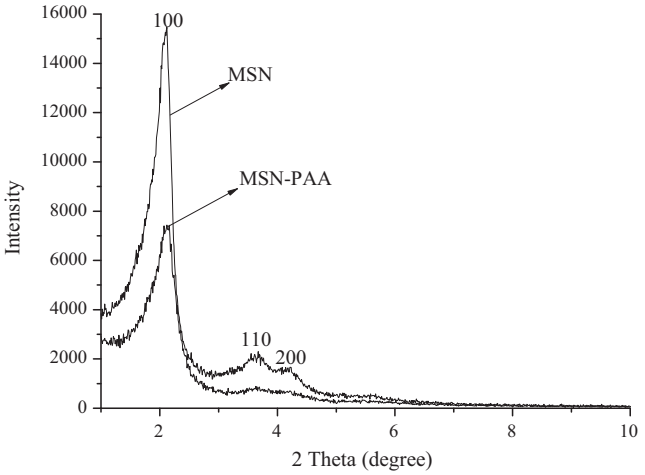

Fig. 2. Low angle powder XRD patterns of MSNs and MSNs–PAA.

Fig. 3 shows the FT-IR spectra of SN-CTAB, MSNs, and MSNs–PAA, respectively. As seen from In the FT-IR spectrum of SN-CTAB, the stretching vibration absorption of C–H from CTAB is at 2922, 2853, and 1482 cm^{-1}, respectively. After a removal of process, these peaks disappeared, shown in the FT-IR spectrum of MSNs, indicating that no residual CTAB existed in the MSNs, and the impact of the toxicity for human health from CTAB was also eliminated. The peaks at 1000 – 1200 and 800/460 cm^{-1} corresponds to stretching and bending vibration absorption of Si–O–Si groups of MSNs, respectively. The absorption of Si–O–Si groups in MSNs still existed after modification with PAA layers, indicating the mesoporous structure of MSNs would remain after the process of modification. For the MSNs–PAA, the characteristic absorption bands at 1723 cm^{-1} appeared compared with MSNs, which could be assigned to the absorption of carboxyl groups of PAA, while the bands at 1530 and 1451 cm^{-1} could be assigned to asymmetric and symmetric stretching vibrations of COO— anion groups, respectively. From these results, it is assumed that PAA layers were grafted successfully onto the surface of MSNs.

Fig. 4 displays TGA data of SN-CTAB, MSNs and MSNs–PAA. As is known to all that silica materials can endure high temperature and all the weight loss should be caused by organic compounds. Thus, the TGA of three samples were carried out from 100 °C. It can be seen that the weight loss at about 100–330 °C for the SN-CTAB was due to desorption of the CTAB. The weight loss at about 100–500 °C for MSNs–PAA may be desorption of the PAA layers on the surface of MSNs. For the MSNs, there is a little weight loss occurring at higher temperatures, which may be due to desorption of the MPS.

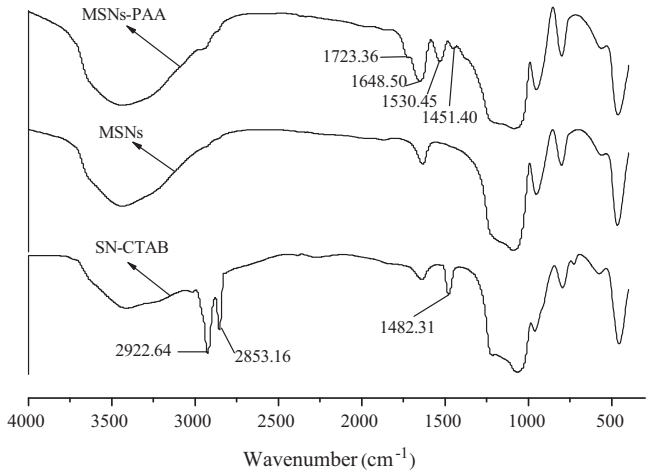

Fig. 3. FT-IR spectra of silica SN-CTAB, MSNs, and MSNs–PAA.

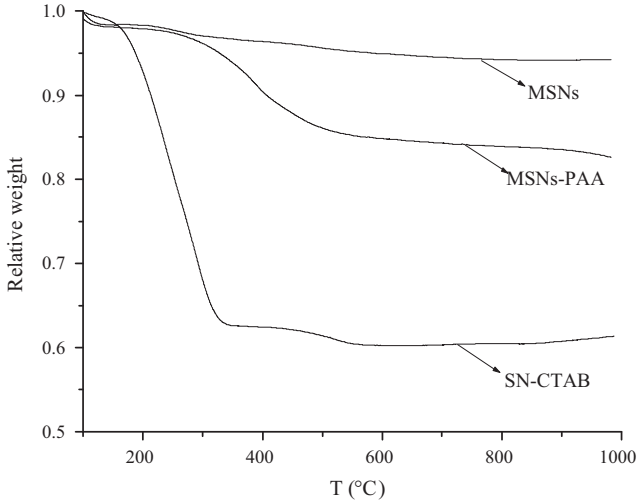

Fig. 4. TGA curves of s SN-CTAB, MSNs, and MSNs–PAA.

Fig. 5 shows both the SEM images and EDS spectra of MSNs and MSNs–PAA. The MSNs had regular shape and good dispersion with some nanopores on the surface (Fig. 5(A)). However, after modification with PAA layers, it can be clearly observed that the powders seem to stick together with irregular shape (Fig. 5(C)). Elemental compositions of the Si (73.69%) and O (26.31%) were observed for MSNs (Fig. 5(B)). After being modified by PAA layers, the contents of Si (65.22%) and O (19.10%) elements were decreased, and a new peak assigned to C appeared with content of 15.68% (Fig. 5(D)). All these results proved that PAA grafted successfully onto the MSNs.

Fig. 6 shows the size distribution of MSNs and MSNs–PAA. As seen, the average size was 396.3–442.7 nm for MSNs and MSNs–PAA, respectively. The reasons of size increasing may be due to the layers of PAA on the surface of MSNs and MSNs–PAA adhesion easier than MSNs. Meanwhile, the HRTEM images gave direct information of the pore structures of MSNs and MSNs–PAA. As seen in Fig. 7(A), the MSNs are uniform nanospheres with regular array of structure channels. There is a PAA layer around the exterior surface of the MSNs–PAA, as shown in Fig. 7(B). The observed parallel channels in the core area still remained, which indicated that the MCM-41 type cylindrical channel-like mesoporous structure of MSNs was not destroyed during the polymerization process.

3.3. EE and LC of salidroside in MSNs–PAA

As the active component, salidroside was used as the guest molecules and loaded into MSNs–PAA. The LC and EE in pH 8.0 PBS solutions were 21.11 μg/mg and 25.33%, respectively. As the control, the loading experiment of MSNs–PAA was also carried out in the pH 1.2 PBS solutions, the LC (3.62 μg/mg) and EE (4.34%) was far lower than that of in pH 8.0 PBS solutions. The pK_a of PAA is 4.5 (Song et al., 2007), so the carboxylate groups of PAA on the surface of MSNs were deprotonated and then became soluble in relatively high pH 8.0 solutions, forming an opened state (Fig. 1). Salidroside could enter into the MSNs easily via opened state in pH 8.0 PBS solutions. On the contrary, the carboxylate groups were protonated in lower pH solution (pH 1.2), the PAA layers were insoluble and were collapsed onto the surface of MSNs, forming a closed state. This hindered salidroside to enter into MSNs–PAA and thus resulted in low loading capacity in pH 1.2 solutions.

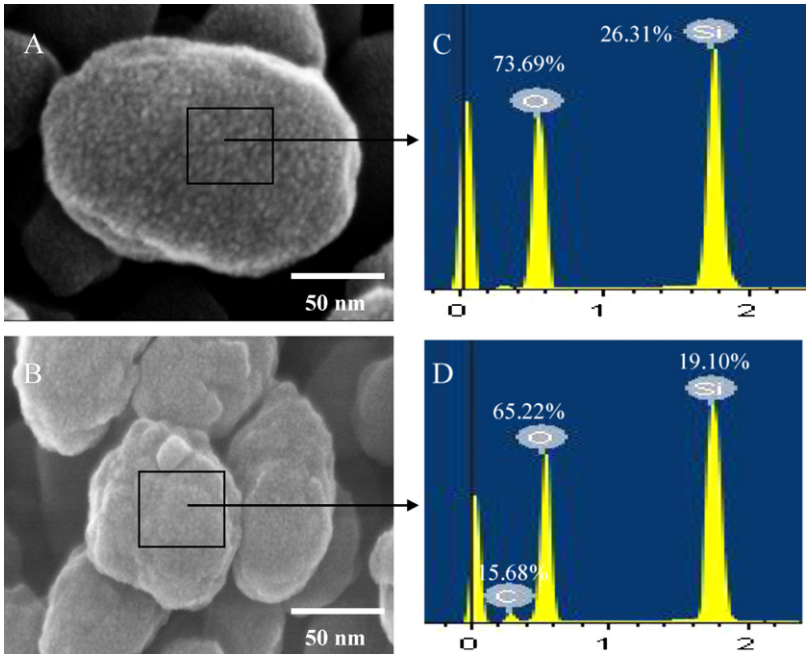

Fig. 5. SEM images and EDS spectra of MSNs (A, C) and MSNs–PAA (B, D).

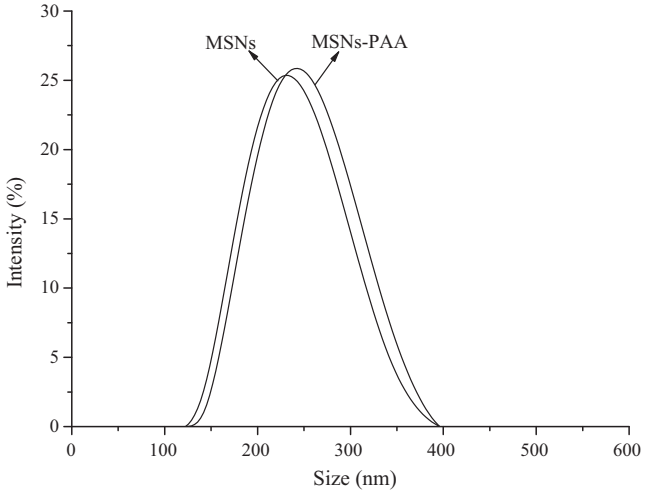

Fig. 6. Size distribution of MSNs and MSNs–PAA.

3.4. In vitro release and release kinetics of MSNs–PAA

Fig. 8(A) shows the in vitro release of salidroside from pure MSNs and MSNs–PAA in pH 1.2 and 8.0 PBS solutions. The results revealed that there were two stages for the release of salidroside from MSNs. The first stage of release was initially rapid, which may be due to the rapid diffusion of the salidroside onto the surface of MSNs. Later, the second stage of release was slow from MSNs. The amounts of release of salidroside from pure-MSNs were higher than that of MSNs–PAA in PBS solutions. The amounts of released salidroside from pure-MSNs in pH 1.2 PBS solutions was about 37.24% for 3 h and 91.65% for 24 h, and the released amounts in pH 8.0 PBS solutions were around 33.67% for 3 h and 83.68% for 24 h, respectively. Comparing to pure-MSNs, the amounts of released salidroside from MSNs–PAA were controlled with pH values. The release amounts of salidroside from MSNs–PAA in pH 8.0 solutions were about 81.45% after 24 h, however, they were only 34.33% in pH 1.2 solutions. In pH 8.0 solutions, the opened state of PAA on the surface of MSNs rendered salidroside accessible to the entrances of pores and the release of salidroside from MSNs–PAA into solutions

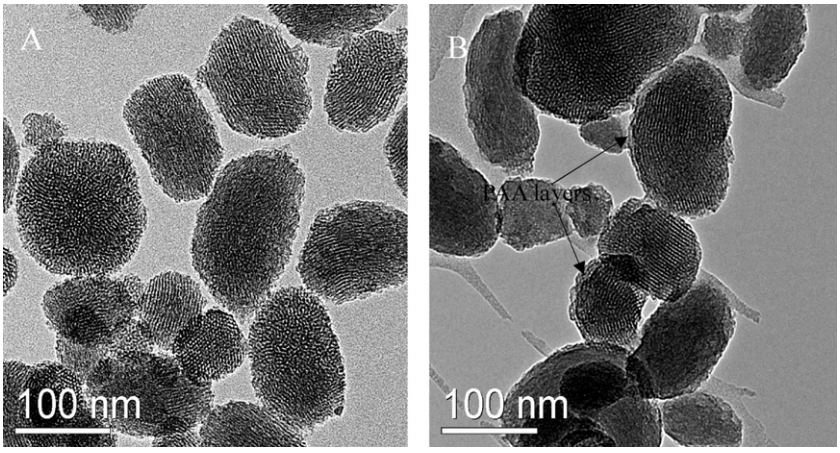

Fig. 7. TEM of MSNs (A) and MSNs–PAA (B).

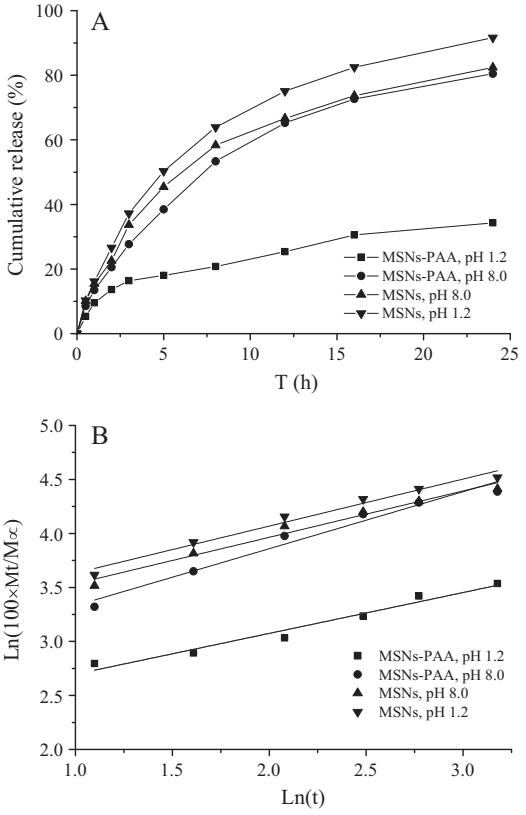

Fig. 8. In vitro release profiles (A) and release kinetics (B) of salidroside from pure MSNs and MSNs–PAA in pH 1.2 and pH 8.0 PBS solutions.

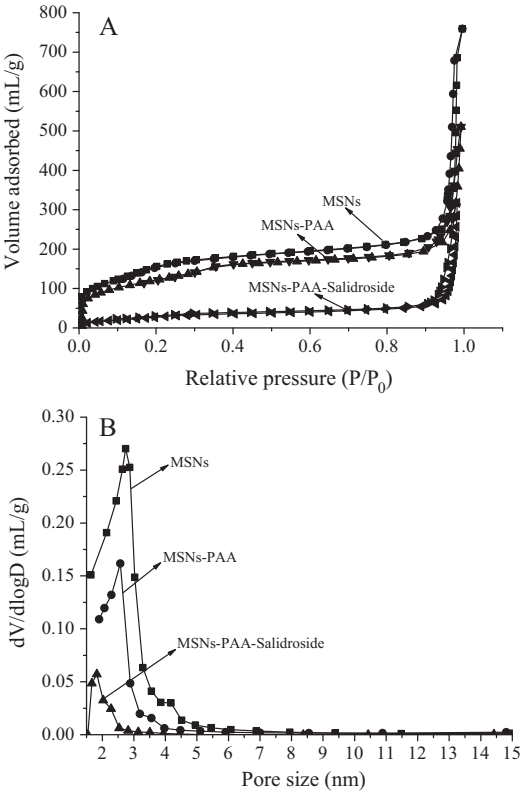

Fig. 9. The N_2 adsorption–desorption isotherms (A) and the corresponding pore size distribution (B) of MSNs, MSNs–PAA and MSNs–PAA after loading (MSNs–PAA–salidroside).

easily. However, in pH 1.2 PBS solutions, the closed state of PAA on the surface of MSNs blocked the pore entrances, and the release of salidroside from the pores of MSNs–PAA was obstructed. Consequently, lower amounts release of salidrodide from MSNs–PAA was observed in pH 1.2 PBS solutions. These results indicated that the pH-responsive PAA layers on the surface of MSNs could effectively regulate the uptake and release of salidroside from MSNs–PAA.

MSNs could be considered as non-swellable spherical sample, and the release kinetics was fitted with Peppas model for the second release stage of MSNs, as shown in Fig. 8(B). The value of n gives an indication of the release mechanism for Peppas model, for example, $n = 0.43$ for typical Fickian diffusion, $n = 0.85$ for erosion transport, and $0.43 < n < 0.85$ for non-typical Fickian transport (Ritger and Peppas, 1987). As seen in Fig. 8(B), the calculated n value of pure MSNs was 0.43 and 0.44 in pH 8.0 and pH 1.2 PBS solutions, respectively. The results indicated that salidroside release from pure-MSNs was driven by the concentration gradient of salidroside and typical Fickian diffusion was the main release mechanism. However, the n value of MSNs–PAA was 0.53 and 0.38 in pH 8.0 and pH 1.2 PBS solutions, respectively (Fig. 8(B)). The results indicated that the non-typical Fickian diffusion was the main release mechanism for MSNs–PAA, which may be due to the swelling and gel state of PAA on the surface of MSNs.

3.5. Nitrogen adsorption–desorption isotherms

The nitrogen adsorption–desorption isotherms and pore size distribution of MSNs samples were shown in Fig. 9. The type IV isotherm curve with a loop was observed for MSNs and MSNs–PAA samples (Fig. 9(A)), which indicated that MSNs and MSNs–PAA possessed a well-defined and MCM-41 type mesoporous structures. The structure parameters of MSNs and MSNs–PAA were listed in Table 1. The surface area, pore volume and peak pore size of MSNs were 505.22 m^2/g, 1.18 cm^3/g and 2.77 nm, respectively. Actually, these parameters of MSNs–PAA were 490.87 m^2/g, 0.82 cm^3/g and 2.56 nm (Table 1). It was observed that there was a little difference in nitrogen adsorption and structure parameters between MSNs and MSNs–PAA, proving that a nano-layer of PAA was exclusively grafted on the external surface of MSNs. The amount of nitrogen adsorption and structure parameters was decreased greatly after loading salidroside into MSNs–PAA. The surface area and pore volume were 88.27 m^2/g and 0.55 cm^3/g, respectively, and correspondingly, the peak pore size decreased from 2.77 to 1.83 nm (Table 1). These results indicated that a large number of salidroside had entered into the MSNs–PAA, and predominantly occupied the pores and channels.

Table 1
The structure parameters of MSNs, MSNs–PAA, and MSNs–PAA after loading salidroside (MSNs–PAA–salidroside).

Samples	BET surface area (m^2/g)	Pore volume (mL/g)	Peak pore diameter (nm)
MSNs	505.22	1.18	2.77
MSNs–PAA	490.87	0.82	2.56
MSNs–PAA–Salidroside	88.27	0.55	1.83

4. Conclusion

A pH-responsive nano-carrier (MSNs–PAA) was successfully developed by using PAA as shell and MSNs as core via seeded precipitation polymerization method. The MSNs–PAA can serve as a novel nano-carrier for loading bioactive molecules of salidroside. The PAA layers on the surface of MSNs could be reversibly opened and closed triggered by pH, and thereby could regulate the uptake and release of salidroside from MSNs. On the other hand, the

biological activity of salidroside could be protected from unfavorable environments by the silica skeleton structure of MSNs. Thus, this nano-carrier maybe has a potential application in delivery system for drugs.

Acknowledgements

This work was supported by the National Natural Science Foundation of China (21201098, 31160317, 21275158, 21105117), the Specialized Research Fund for the Doctoral Program of Higher Education (20113601110004), and the 100 Talents Program of the Chinese Academy of Sciences.

References

Cui, D.C., Lu, W.L., Sa Er, A., Gu, M.J., Lu, X.J., Fan, T.Y., 2012. Poly(acrylic acid) microspheres loaded with lidocaine: preparation and characterization for arterial embolization. Int. J. Parasitol. 436, 527–535.

Dai, Y.L., Zhang, C.M., Cheng, Z.Y., Ma, P.A., Li, C.X., Kang, X.J., Yang, D.M., Lin, J., 2012. pH-responsive drug delivery system based on luminescent CaF_2:Ce^{3+}/Tb^{3+}-poly(acrylic acid) hybrid microspheres. Biomaterials 33, 2583–2592.

De Bock, K., Eijnde, B.O., Ramaekers, M., Hespel, P., 2004. Acute *Rhodiola rosea* intake can improve endurance exercise performance. Int. J. Sport Nutr. Exerc. Metab. 14, 298–307.

Fan, M.H., Xu, S.Y., Xia, S.Q., Zhang, X.M., 2007. Effect of different preparation methods on physicochemical properties of salidroside liposomes. J. Agric. Food Chem. 55, 3089–3095.

Fathi, M., Mozafari, M.R., Mohebbi, M., 2012. Nanoencapsulation of food ingredients using lipid based delivery systems. Trends Food Sci. Technol. 23, 13–27.

Fleige, E., Quadir, M.A., Haag, R., 2012. Stimuli-responsive polymeric nanocarriers for the controlled transport of active compounds: concepts and applications. Adv. Drug Deliv. Rev. 64, 866–884.

Fleming, M.S., Mandal, T.K., Walt, D.R., 2001. Nanosphere-microsphere assembly: methods for core–shell materials preparation. Chem. Mater. 13, 2210–2216.

Gao, Q., Xu, Y., Wu, D., Shen, W.L., Deng, F., 2010. Synthesis, characterization, and in vitro pH-controllable drug release from mesoporous silica spheres with switchable gates. Langmuir 26, 17133–17138.

Giri, S., Trewyn, B.G., Stellmaker, M.P., Lin, V.S.Y., 2005. Stimuli-responsive controlled-release delivery system based on mesoporous silica nanorods capped with magnetic nanoparticles. Angew. Chem. Int. Ed. 44, 5038–5044.

Hasanzadeh, M., Shadjou, N., Guardia, M., Eskandani, M., Sheikhzadeh, P., 2012. Mesoporous silica-based materials for use in biosensors. Trends Anal. Chem. 33, 117–129.

Hong, C.Y., Li, X., Pan, C.Y., 2009. Fabrication of smart nanostructure with a mesoporous core and a pH-responsive shell for controlled uptake and release. J. Mater. Chem. 15, 5155–5160.

Hu, X.L., Zhang, X.Q., Qiu, S.F., Yu, D.H., Lin, S.X., 2010. Salidroside induces cell-cycle arrest and apoptosis in human breast cancer cells. Biochem. Biophys. Res. Commun. 398, 62–67.

Jones, C.D., Lyon, L.A., 2000. Synthesis and characterization of multiresponsive core–shell microgels. Macromolecules 33, 8301–8306.

Kim, T., Momin, E., Choi, J., Yuan, K., Zaidi, H., Kim, J., Park, M., Lee, N., McMahon, M.T., Hinojosa, A.Q., Bulte, J.W.M., Hyeon, T., Gilad, A.A., 2011a. Mesoporous silica-coated hollow manganese oxide nanoparticles as positive t_1 contrast agents for labeling and MRI tracking of adipose-derived mesenchymal stem cells. J. Am. Chem. Soc. 133, 2955–2961.

Kim, T.W., Slowing, I.I., Chung, P.W., Lin, V.S.Y., 2011b. Ordered mesoporous polymer-silica hybrid nanoparticles as vehicles for the intracellular controlled release of macromolecules. ACS Nano 5, 360–366.

Lai, C.Y., Trewyn, B.G., Jeftinija, D.M., Jeftinija, K., Xu, S., Jeftinija, S., Lin, V.S.Y., 2003. A mesoporous silica nanosphere-based carrier system with chemically removable cds nanoparticle caps for stimuli-responsive controlled release of neurotransmitters and drug molecules. J. Am. Chem. Soc. 125, 4451–4459.

Leung, K.C.F., Nguyen, T.D., Stoddart, J.F., Zink, J.I., 2006. Supramolecular nanovalves controlled by proton abstraction and competitive bingding. Chem. Mater. 18, 5919–5928.

Lin, C.H., Cheng, S.H., Liao, W.N., Wei, P.R., Sung, P.J., Weng, C.F., Chia-Hung Lee, C.H., 2012. Mesoporous silica nanoparticles for the improved anticancer efficacy of cisplatin. Int. J. Pharm. 429, 138–147.

Lin, J.H., Wei, Z.J., Mao, C.M., 2011. A label-free immunosensor based on modified mesoporous silica for simultaneous determination of tumor markers. Biosens. Bioelectron. 29, 40–45.

Liu, Y.Y., Fan, X.D., Wei, B.R., Si, Q.F., Chen, W.X., Sun, L., 2006. pH-responsive amphiphilic hydrogel networks with IPN structure: a strategy for controlled drug release. Int. J. Pharm. 308, 205–209.

Nguyen, T.D., Liu, Y., Saha, S., Leung, K.C.F., Stoddart, J.F., Zink, J.I., 2007. Design and optimization of molecular nanovalves based on redox-switchable bistable rotaxanes. J. Am. Chem. Soc. 129, 626–634.

Park, I.Y., Kim, I.Y., Yoo, M.K., Choi, Y.J., Cho, M.H., Cho, C.S., 2008. Mannosylated polyethylenimine coupled mesoporous silica nanoparticles for receptor mediated gene delivery. Int. J. Pharm. 359, 280–287.

Ritger, P.L., Peppas, N.A., 1987. A simple equation for description of solute release II Fickian and anomalous release from swellable devices. J. Control. Release 5, 37–42.

Rodin, I.A., Stavrianidi, A.N., Braun, A.V., Shpigun, O.A., Popik, M.V., 2012. Simultaneous determination of salidroside, rosavin, and rosarin in extracts from *Rhodiola rosea* by high performance liquid chromatography with tandem mass spectrometry detection. J. Anal. Chem. 67, 1026–1030.

Slowing, I.I., Trewyn, B.G., Giri, S., Lin, V.S.Y., 2007. Mesoporous silica nanoparticles for drug delivery and biosensing applications. Adv. Funct. Mater. 17, 1225–1236.

Slowing, I.I., Vivero-Escoto, J.L., Wu, C.W., Lin, V.S.Y., 2008. Mesoporous silica nanoparticles as controlled release drug delivery and gene transfection carriers. Adv. Drug Deliv. Rev. 60, 1278–1288.

Song, S.W., Hidajat, K., Kawi, S., 2007. pH-Controllable drug release using hydrogel encapsulated mesoporous silica. Chem. Commun., 4396–4398.

Taillefer, J., Jones, C., Brasseur, C., Vanlier, J.E., Leroux, J.C., 2000. Preparation and characterization of pH-responsive polymeric micelles for the delivery of photosensitizing anticancer drugs. J. Pharm. Sci. 89, 52–62.

Tang, H.Y., Guo, J., Sun, Y., Chang, B.S., Ren, Q.G., Yang, W.L., 2011. Facile synthesis of pH sensitive polymer-coated mesoporous silica nanoparticles and their application in drug delivery. Int. J. Pharm. 421, 388–396.

Tasbihi, M., Štangar, U.L., Černigoj, U., Jirkovsky, J., Bakardjieva, S., Tušar, N.N., 2011. Photocatalytic oxidation of gaseous toluene on titania/mesoporous silica powders in a fluidized-bed reactor. Catal. Today 161, 181–188.

Thomas, M.J.K., Slipper, I., Walunj, A., Jain, A., Favretto, M.E., Kallinteri, P., Douroumis, D., 2010. Inclusion of poorly soluble drugs in highly ordered mesoporous silica nanoparticles. Int. J. Pharm. 387, 272–277.

Torney, F., Trewyn, B.G., Lin, V.S.Y., Wang, K., 2007. Mesoporous silica nanoparticles deliver DNA and chemicals into plants. Nat. Nanotechnol. 2, 295–300.

You, Y.Z., Kalebaila, K.K., Brock, S.L., Oupicky, D., 2008. Temperature-controlled uptake and release in PNIPAM-modified porous silica nanoparticles. Chem. Mater. 20, 3354–3359.

Wang, G.Q., Wang, Y.Q., Chen, L.X., Choo, J.B., 2011a. Mesoporous silica-coated gold nanorods: towards sensitive colorimetric sensing of ascorbic acid via target-induced silver overcoating. Nanoscale 3, 1756–1759.

Wang, G.Q., Chen, Z.P., Wang, W.H., Yan, B., Chen, L.X., 2011b. Chemical redox-regulated mesoporous silica-coated gold nanorods for colorimetric probing of Hg^{2+} and S^{2-}. Analyst 136, 174–178.

Wang, H.B., Ding, Y.Y., Zhou, J., Sun, X.L., Siwang Wang, S.W., 2009. The in vitro and in vivo antiviral effects of salidroside from *Rhodiola rosea* L. against coxsackievirus B3. Phytomedicine 6, 146–155.

Wang, R., Yu, C.W., Yu, F.B., Chen, L.X., 2010. Molecular fluorescent probes for monitoring pH changes in living cells. Trends Anal. Chem. 29, 1004–1013.

Xu, S.F., Chen, L.X., Li, J.H., Qin, W., Ma, J.P., 2011. Preparation of hollow porous molecularly imprinted polymers and their applications to solid-phase extraction of triazines in soil samples. J. Mater. Chem. 21, 12047–12053.

Zhang, L., Yu, H.X., Sun, Y., Lin, X.F., Chen, B., Tan, T., Cao, G.X., Wang, Z.W., 2007. Protective effects of salidroside on hydrogen peroxide-induced apoptosis in SH-SY5Y human neuroblastoma cells. Eur. J. Pharmacol. 564, 18–25.

Zhang, L., Yu, H.X., Zhao, X.C., Lin, X.F., Tan, C., Cao, G.X., Wang, Z.W., 2010. Neuroprotective effects of salidroside against beta-amyloid-induced oxidative stress in SH-SY5Y human neuroblastoma cells. Neurochem. Int. 57, 547–555.

Zhang, Z., Xu, S.F., Li, J.H., Xiong, H., Peng, H.L., Chen, L.X., 2012. Selective solid-phase extraction of Sudan I in chilli sauce by single-hole hollow molecularly imprinted polymers. J. Agric. Food Chem. 60, 180–187.